Local Structural Plasticity of the Prion Protein. Analysis of NMR Relaxation Dynamics[†]

John H. Viles,[‡,§] David Donne,[‡] Gerard Kroon,[‡] Stanley B. Prusiner,[||] Fred E. Cohen,[||] H. Jane Dyson,*[,‡] and Peter E. Wright*[,‡]

Department of Molecular Biology and Skaggs Institute for Chemical Biology, The Scripps Research Institute, La Jolla, California 92037, and Departments of Neurology, Pharmaceutical Chemistry, Cellular and Molecular Pharmacology, Medicine, Biochemistry, and Biophysics, The University of California, San Francisco, California 94143

Received December 20, 2000

ABSTRACT: A template-assisted conformational change of the cellular prion protein (PrP^C) from a predominantly helical structure to an amyloid-type structure with a higher proportion of β-sheet is thought to be the causative factor in prion diseases. Since flexibility of the polypeptide is likely to contribute to the ability of PrP^C to undergo the conformational change that leads to the infective state, we have undertaken a comprehensive examination of the dynamics of two recombinant Syrian hamster PrP fragments, PrP(29−231) and PrP(90−231), using ^{15}N NMR relaxation measurements. The molecular motions of these PrP fragments have been studied in solution using ^{15}N longitudinal (T_1) and transverse relaxation (T_2) measurements as well as $\{^1H\}-^{15}N$ nuclear Overhauser effects (NOE). These data have been analyzed using both reduced spectral density mapping and the Lipari−Szabo model free formalism. The relaxation properties of the common regions of PrP(29−231) and PrP(90−231) are very similar; both have a relatively inflexible globular domain (residues 128−227) with a highly flexible and largely unstructured N-terminal domain. Residues 29−89 of PrP(29−231), which include the copper-binding octarepeat sequences, are also highly flexible. Analysis of the spectral densities at each residue indicates that even within the structured core of PrP^C, a markedly diverse range of motions is observed, consistent with the inherent plasticity of the protein. The central portions of helices B and C form a relatively rigid core, which is stabilized by the presence of an interhelix disulfide bond. Of the remainder of the globular domain, the parts that are not in direct contact with the rigid region, including helix A, are more flexible. Most significantly, slow conformational fluctuations on a millisecond to microsecond time scale are observed for the small β-sheet. These results are consistent with the hypothesis that the infectious, scrapie form of the protein PrP^{Sc} could contain a helical core consisting of helices B and C, similar in structure to the cellular form PrP^C. Our results indicate that residues 90−140, which are required for prion infectivity, are relatively flexible in PrP^C, consistent with a lowered thermodynamic barrier to a template-assisted conformational change to the infectious β-sheet-rich scrapie isoform.

Prion diseases include scrapie in sheep and bovine spongiform encephalopathy in cattle, as well as Creutzfeldt-Jakob disease (CJD), Gerstmann-Sträussler-Scheinker syndrome (GSS), fatal insomnia (FI), and kuru of humans (*1*−*3*). A new variant form of CJD has been reported which is thought to be caused by the ingestion of infected beef (*4*, *5*). Prions are distinct from bacteria, viruses, and viroids in that the infectious pathogen contains no nucleic acid. The infectious prion consists of a post-translationally modified form of the prion protein known as PrP^{Sc} [1] (*6*, *7*). The sequences of PrP^{Sc} and the noninfectious cellular precursor PrP^C are identical (*8*). However, the two forms of the protein differ dramatically in their secondary and tertiary structures (*9*, *10*).

The prion protein (PrP) is composed of approximately 250 amino acids and is encoded by a single-copy chromosomal gene. The 22 N-terminal residues consist of a signal sequence, and the C-terminal residue has a glycosylphosphatidylinositol (GPI) membrane anchor. Native PrP^C contains two N-linked glycosylation sites. Structural information about a number of mammalian PrP^C protein constructs, obtained by overexpression in bacteria, has been reported. These constructs consist of fragments of varying lengths, including residues 121−231, residues 90−231, residues 29−231, and residues 23−231. Crystallographic data are not

[†] This work was supported by Grant NS14069 from the National Institutes of Health.

* To whom correspondence should be addressed: Department of Molecular Biology, The Scripps Research Institute, MB-2, 10550 N. Torrey Pines Rd., La Jolla, CA 92037. Telephone: (858) 784-9721. Fax: (858) 784-9822. E-mail: wright@scripps.edu or dyson@scripps.edu.

[‡] The Scripps Research Institute.

[§] Present address: School of Biological Sciences, Queen Mary College, University of London, Mile End Road, London E1 4NS, U.K.

[||] The University of California.

[1] Abbreviations: PrP, prion protein; PrP^{Sc}, scrapie isoform of PrP; PrP^C, cellular isoform of PrP; PrP27−30, protease resistant core of PrP^{Sc} containing residues 90−231; Mo, mouse; SHa, Syrian hamster; GPI, glycosylphosphatidylinositol; BSE, bovine spongiform encephalopathy; CD, circular dichroism; FTIR, Fourier transform infrared; HSQC, heteronuclear single-quantum coherence; NOE, nuclear Overhauser effect; GdnHCl, guanidinium hydrochloride.

10.1021/bi002898a CCC: $20.00
Published on Web 02/08/2001

available for any of these fragments. The shortest fragment, obtained for the mouse system [MoPrP(121−231)], was characterized structurally by NMR (*11*) and was shown to consist of a folded domain containing three helices and two short β-strands. A solution structure was also calculated for the shortest fragment that is capable of forming PrP^{Sc}, from the Syrian hamster system [SHaPrP(90−231)] (*12*), and parallel structural information was obtained by NMR for the longer construct of the Syrian hamster protein, SHaPrP(29−231) (*13*), and the mouse protein MoPrP(23−231) (*14*), representing the entire operative polypeptide sequence of the prion gene product. The structure of the analogous human protein HuPrP(23−231) has now also been reported (*15*). It is clear from all of these studies that the prion protein consists under these conditions of a structured domain corresponding approximately to residues 121−231 and an unstructured domain at the N-terminus.

Much less is known about the conformation of PrP^{Sc}, one form of which is protease-resistant and largely insoluble. Thin film CD and FTIR studies indicate some reduction in helical content relative to that of PrP^{C} (from 42 to 30%), while the β-sheet content increases from around 3% in PrP^{C} to between 34 and 43% in full-length PrP^{Sc} (*9*, *10*). It is believed that formation of PrP^{Sc} and of subsequent amyloid arises from the PrP^{Sc} acting as a template to induce or stabilize a conformational switch in PrP^{C} in the presence of a chaperone known as protein X (*16*). The structural transition between such forms would presumably be made easier if the globular structure of the domain has low stability or if, as is the case with PrP, part of the domain is unstructured. Nevertheless, in the PrP^{Sc} form, helical structure is lost and β-structure is gained; this implies that parts of the structured domain of PrP^{C} must change structure. It is the aim of this work to ascertain if there are regions within the structured domain of PrP^{C} that exhibit local high flexibility. This would indicate a lower energy barrier to structural rearrangement. We also wanted to determine whether the length of the unstructured tail has any influence on either the dynamics of the tail itself or that of parts of the structured domain. Hence, we undertook a detailed study of the dynamics of two prion protein fragments from Syrian hamster, SHaPrP(29−231) and SHaPrP(90−231), using NMR relaxation measurements.

MATERIALS AND METHODS

Protein Expression and Purification. ^{15}N-enriched recombinant Syrian hamster PrP(29−231) and PrP(90−231) were expressed in *Escherichia coli*, purified, and refolded as previously described (*13*, *17*). For NMR experiments, the protein concentration was 0.5 mM at pH 5.5 in 50 mM sodium acetate buffer. Sodium azide (0.05%) was added to inhibit bacterial growth.

NMR Spectroscopy. NMR experiments were performed on Bruker AMX-II and DRX spectrometers operating at 500 and 600 MHz ^{1}H frequencies, respectively, i.e., at 50.7 and 60.8 MHz ^{15}N frequencies, respectively. All relaxation measurements were performed at 30 °C, with the probe temperature calibrated using methanol (*18*). The pulse sequences used to obtain T_1, T_2, and heteronuclear NOE spectra are those described by Farrow et al. (*19*), who employed gradient selection and sensitivity enhancement, as well as minimal water suppression.

Typically, 10 time points were collected for T_1 and T_2 experiments, and each set included at least two duplicate measurements to allow estimation of the uncertainty. The delays that were used were as follows: 600 MHz for PrP(29−231), T_1 delays of 10, 10, 130, 290, 490, 490, 730, 1050, 1050, 1510, 2290, and 3000 ms and T_2 delays of 6, 6, 22, 42, 70, 70, 102, 182, 182, 262, 382, and 502 ms; 500 MHz for PrP(29−231), T_1 delays of 10, 10, 130, 130, 290, 490, 490, 590, 730, 890, 1050, 1050, 1570, and 2290 ms and T_2 delays of 10, 10, 22, 34, 42, 54, 70, 70, 82, 102, 122, 182, 182, 262, 382, and 502 ms; 500 MHz for PrP(90−231), T_1 delays of 10, 10, 130, 130, 290, 290, 490, 490, 730, 1050, 1050, 1570, and 2290 ms and T_2 delays of 10, 10, 26, 42, 58, 58, 74, 106, 142, 202, 302, and 422 ms. Repeated numbers indicate duplicate measurements.

$\{^{1}H\}-^{15}N$ heteronuclear NOE spectra were recorded for PrP(29−231) at both 500 and 600 MHz; each spectrum was measured four times. A single NOE spectrum was recorded at 500 MHz for PrP(90−231). In the direct dimension (^{1}H), the carrier frequency was set on the water resonance with a spectral width of 15 ppm; the indirect (^{15}N) dimension was centered at 118 ppm with a spectral width of 25 ppm. Two thousand complex data points with 128 complex increments were collected. Typical T_1 experiments were acquired with 24 scans and a repetition delay of $3T_1$ s, while T_2 experiments were acquired with 32 scans and a 500 μs delay between 180 pulses in the Carr−Purcell−Meiboom−Gill (CPMG) pulse train. Each $\{^{1}H\}-^{15}N$ NOE spectrum (both saturated and nonsaturated pairs) was acquired with 48 scans. The ^{1}H saturation was achieved by the application of 120° ^{1}H pulses separated by 18 ms, for a 3 s period. In addition, a 3 s recycle delay was employed.

Off-resonance $T_{1\rho}$ relaxation times were measured at 600 MHz using a modification of the method of Zinn-Justin et al. (*20*), with a 4 ms adiabatic pulse at the beginning and end of the spin lock period. Data were acquired with a spectral width of 9615.38 Hz in the ^{1}H dimension (1024 complex points) and 1562.5 Hz in the ^{15}N dimension (128 complex points). Water suppression was accomplished using water flip back in conjunction with a zz-filter. Relaxation decay curves were sampled using spin lock periods of 10, 30, 50, 50, 80, 100, 150, and 200 ms. The off-resonance rf field was placed to give spin lock field strengths of 1.211, 1.307, 1.494, 1.883, 2.077, 2.474, 2.671, and 3.072 kHz at the center of the ^{15}N spectrum.

Data Processing. All spectra were processed in an identical fashion using Felix95/97 software (MSI). Spectra were zero filled to 4K and 1K points in the t_2 and t_1 dimensions, respectively, and were apodized using a phase-shifted Gaussian function. The residual water signal was removed using a low-frequency filter. Cross-peak intensity was measured as peak height rather than volume, to minimize the problem of peak overlap. A search routine (more than $\pm$3 data points) for each peak was used within Felix to find the position of the peak maxima. In the case of resonances associated with the octarepeat region, peak volumes were measured, as it was found that the multiple degenerate peaks in the octarepeat region gave poorly defined peak maxima.

The exponential decay curves for T_1 and T_2 peak intensities were fitted to the two-parameter fit $I(t) = I_0e^{-t/T_n}$ or the three-parameter fit $I(t) = I_\infty + I_0e^{-t/T_n}$, where I is the intensity, t is the delay in CPMG or longitudinal delay, and T_n is T_1 or T_2 value (*21*). Two-parameter fits were used for the majority of the residues for both T_1 and T_2 data. In the case of a limited number of residues with weak N−H cross-peaks (typically five residues for each data set), a three-parameter fit was used. Weak peaks were defined as those with an initial intensity less than 15 times the standard error associated with the measurement of peak intensity. The standard error was determined via repeat measurement for a number of time points in the decay curve. The heteronuclear NOE values were obtained from the ratio of peak intensity for ^{1}H-saturated and unsaturated spectra. The error in the heteronuclear NOE $\{^1H\}-^{15}N$ data was determined from four repeat measurements. In the case of PrP(90−231), where only one data set was acquired at 500 MHz, an estimate of the error was obtained from the noise in the baseline, according to the method of Farrow et al. (*19*).

Model Free Analysis and Spectral Density Functions. Model free analysis was performed using ModelFree 3.1 (kindly provided by A. Palmer, Columbia University, New York, NY) using protocols adapted from Mandel et al. (*22*). Reduced spectral density mapping, assuming a single spectral density for $J(\omega_H+\omega_N)$, $J(\omega_H)$, and $J(\omega_H-\omega_N)$ of $J(0.87\omega_H)$, was carried out as described by Farrow et al. (*23*), using an in-house program. The constant for chemical shift anisotropy was −170 ppm (*24*), and the N−H bond length was 1.02 Å.

Translational Diffusion Measurements. The translational self-diffusion rate D_t was measured using pulsed field gradients in the longitudinal encode−decode (LED) sequence (*25*). Twelve different field gradient strengths were used between 8 and 60% strength (100% gradient strength was approximately 30.4 G/cm). The baseline-corrected integrals of the proton spectra were measured in the aromatic and aliphatic regions. The plot of ln(I) versus G^2 was linear and was fitted to the equation

$$\ln(I) = G^2\gamma^2\delta^2(\Delta/3 - \delta/3)D_t + \ln(I_0)$$

where I is the intensity of the ^{1}H signal, G is the gradient strength in Gauss per centimeter, $\gamma = 26\,753$ rad s^{-1} G^{-1}, δ is the length of the gradient pulse (fixed at 7 ms), Δ is the diffusion time between gradients (fixed at 132.5 ms), and D_t is the translational self-diffusion rate. The translational diffusion rate for the prion samples was obtained from the slope of the line following calibration with a standard lysozyme sample; D_t for lysozyme (2 mM in a $^1H_2O/^2H_2O$ mixture) is 1.08×10^{-6} s^{-1} at 298 K (*25*).

Hydrodynamics Calculations. The hydrodynamics of the PrP core were calculated using the method of Barbato et al. (*26*) with the computer program MASH (I. Radhakrishnan, unpublished), using a 3 Å bead size centered on the Cα atom. The coordinates for the structured core of PrP were obtained from the PDB [1B10 (*12*)].

BACKGROUND THEORY

Reduced spectral density mapping is a convenient method of characterizing the motion of each N−H bond at ω_0, ω_N, and $0.87\omega_H$ frequencies (*27*, *28*). The spectral densities at these three frequencies can be obtained from relaxation rates R_1 ($1/T_1$) and R_2 ($1/T_2$) and the heteronuclear NOE using eqs 1−4.

$$\sigma_{NH} = R_1(\text{NOE} - 1)\gamma_N/\gamma_H \quad (1)$$

$$J(0) = (6R_2 - 3R_1 - 2.72\sigma_{NH})/(3d^2 + 4c^2) \quad (2)$$

$$J(\omega_N) = (4R_1 - 5\sigma_{NH})/(3d^2 + 4c^2) \quad (3)$$

$$J(0.87\omega_H) = 4\sigma_{NH}/(5d^2) \quad (4)$$

where $d = \mu h\gamma_N\gamma_H r^{-3}$ and $c = \omega_N\,\Delta\sigma \times 3^{-1/2}$ (*28*). The $J(0)$ spectral density function is equal to $^2/_5\tau_m$, where τ_m is the rotational correlation time, assuming there are no internal motions. A $J(0)$ value of less than $^2/_5\tau_m$ indicates internal flexibility of the N−H bond; the smaller the value of $J(0)$, the greater the sub-nanosecond flexibility of the N−H bond vector (*29*). Slow micro- to millisecond motions (R_{ex}) can also be reflected in $J(0)$ spectral densities, as an increase in $J(0)$ values. The R_{ex} motions have no effect on $J(\omega_N)$ or $J(\omega_H)$ spectral densities and so may be used to isolate these motions observed in the $J(0)$ spectral densities. Fast picosecond motions are reflected in large high-frequency $J(\omega_H)$ spectral densities. For small proteins, $J(\omega_N)$ will decrease with increased internal flexibility; as protein size increases, this effect becomes less apparent, and for very large proteins, $J(\omega_N)$ will increase with increased flexibility (*29*, *30*).

The model free formalism (*31*, *32*) is often used to describe the motions of a protein in terms of a rotational correlation time (τ_m) and an order parameter (S^2). The order parameter describes the amplitude of the nanosecond time scale motions and can range between 0 and 1.0, representing complete disorder and complete order, respectively. If necessary, additional fast internal motions on the picosecond time scale (τ_e) can be incorporated into the spectral density function used to fit the backbone relaxation data:

$$J(\omega) = {}^2/_5(S^2\tau_m)/\{1 + (\omega^2\tau_m{}^2) + {}^2/_5[(1 - S^2)\tau]/[1 + (\omega\tau)^2]\} \quad (5)$$

where $1/\tau = 1/\tau_m + 1/\tau_e$ and $\tau_m \gg \tau_e$. Slower segmental motions on the milli- to microsecond time-scale (R_{ex}) can also be incorporated, where $R_2(\text{obs}) = R_2 + R_{ex}$. It has also been shown (*33*) that an approximate S^2 can be obtained directly from $J(0)$ and $J(\omega_N)$:

$$S^2 = {}^5/_2[J(0) - J(\omega_N)](1 + \omega_N{}^2\tau_m{}^2)/(\omega_N{}^2\tau_m{}^3) \quad (6)$$

An approximate rotational correlation time (τ_m) and the rotational diffusion rate can be obtained from the ratio of T_1 and T_2 values (*34*):

$$\tau_m = (2\omega_N)^{-1}[(6T_1/T_2) - 7]^{1/2} \quad (7)$$

A trimmed mean T_1/T_2 ratio (*26*) is employed so that only rigid amide nitrogens are used in the calculation of τ_m. In this way, fast internal motions or slow segmental motions should not affect the T_1 and T_2 values used to estimate τ_m. After model selection for each residue, an optimized rotational correlation time (τ_m) can be calculated using the model free formalism.

Alternatively, an effective rotational correlation time ($\tau_{c,i}$) at each residue can also be calculated from $J(0)$ and $J(\omega_N)$

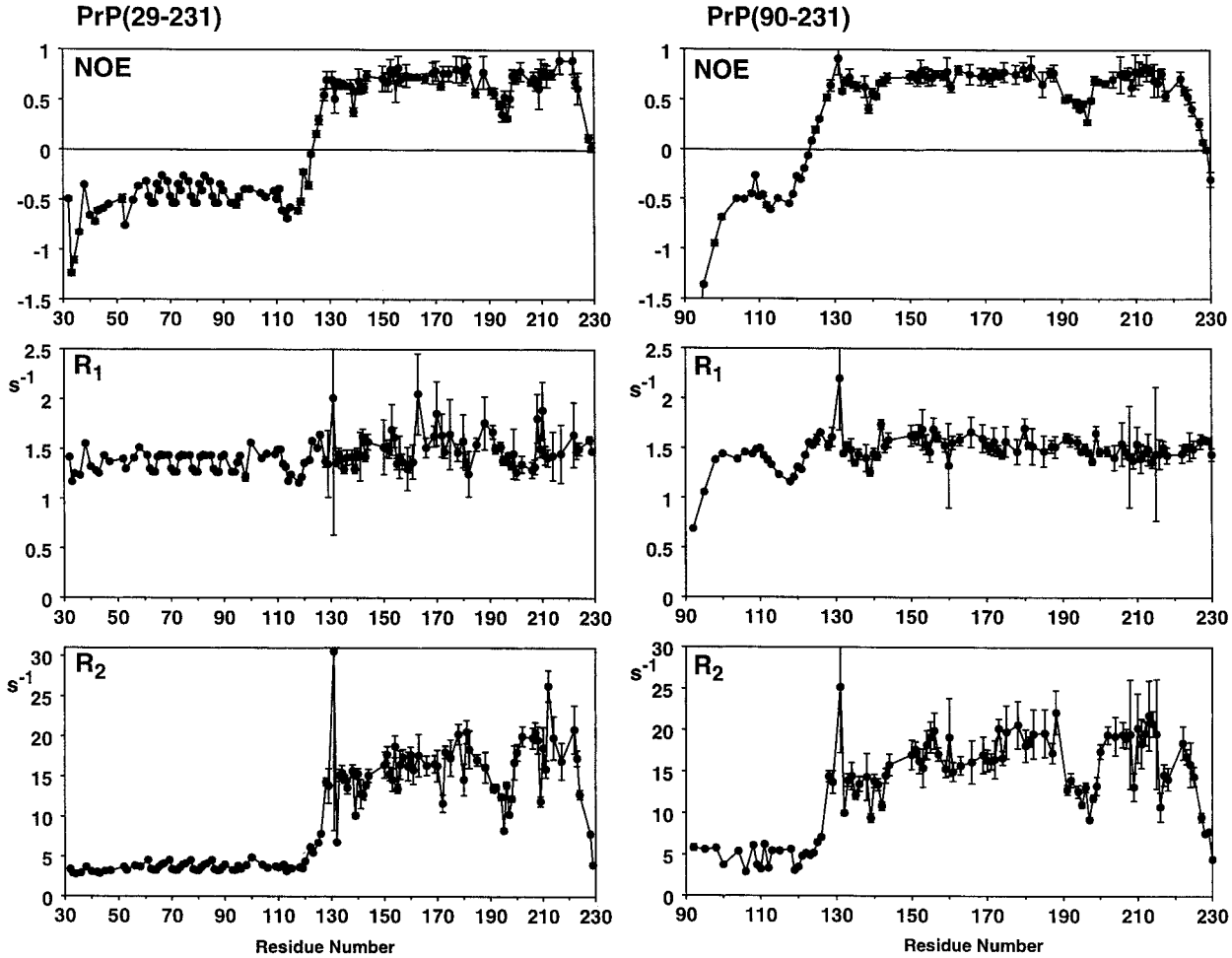

FIGURE 1: Relaxation rates R_1 (=$1/T_1$) and R_2 (=$1/T_2$) and heteronuclear NOE for PrP(29−231) and PrP(90−231) at 500 MHz. Sample conditions: 30 °C, pH 5.5, and 0.1 M acetate buffer.

according to eq 8 (*33*). The $\tau_{c,i}$ for all residues should be the same if there are neither fast internal motions nor slow segmental motions and tumbling is isotropic.

$$\tau_{c,i} = 1/\omega_N\{[J(0)_i - J(\omega_N)_i]/J(\omega_N)_i\}^{1/2} \quad (8)$$

The most widely used model free formalism assumes isotropic tumbling (*31*, *32*). In this case, τ_m is identical for each ^{15}N nucleus. If the protein does not approximate a sphere, then individual τ_m values will vary according to the angle between the N−H bond vector and the long axis of the protein (*35*−*37*).

RESULTS

Relaxation Measurements. To gain insight into the motion of the backbone of PrP in solution, ^{15}N longitudinal (T_1) and transverse (T_2) relaxation times and {^1H}−^{15}N heteronuclear NOEs were measured for two fragments of different lengths, PrP(29−231) and PrP(90−231). The R_1 and R_2 relaxation rates and heteronuclear NOEs for both PrP^C fragments at 500 MHz are shown in Figure 1. Resonance assignments are available for both SHaPrP(29−231) (*13*) and SHaPrP-(90−231) (*12*). Of the 188 N−H resonances for PrP(29−231) (201 minus 13 prolines), 59 cross-peaks were overlapping and were not used in the dynamics analysis. No data are thus presented for the following residues: 30, 31, 37, 41, 48, 49, 57, 96−99, 101, 103, 107, 108, 116, 117, 121, 124, 127, 130, 145−149, 161, 162, 164, 167, 168, 171, 174, 176, 177, 179, 183, 184, 186, 187, 189, 190, 193, 201, 203−205, 213, 215, 216, 218−221, 225−227, 230, and 231. In all, 129 cross-peaks were analyzed for PrP(29−231). For PrP(90−231), 41 cross-peaks were found to be overlapping and were not used, including residues 91, 93, 94, 96, 98, 99, 101, 103, 107, 114, 116, 117, 127, 130, 145−149, 162, 164, 167, 168, 177, 179, 183, 184, 186, 189, 190, 193, 201, 203, 205, 219−221, 226, and 231. A total of 95 of the possible 136 N−H cross-peaks were used in the backbone dynamics analysis of PrP(90−231).

The number of resonances which were not used in the final dynamics analysis is rather high, due to the limited dispersion in the ^1H−^{15}N correlated spectra which occurs as a result of the lack of ordered structure in about half of the residues in PrP(29−231) and about a third of the residues in PrP(90−231). It was found by comparison of relaxation data at two fields for PrP(29−231) that a number of resonances that were initially believed to be adequately separated from neighboring resonances were in fact sufficiently overlapped so that the relaxation behavior of the resonances led them to interfere with each other. The problem of a small degree of overlap of the ^{15}N−^1H HSQC cross-peaks is made worse by the very different relaxation behavior of the resonances of residues from the unstructured N-terminal half of the molecule and the relatively structured C-terminal half. The octarepeat region (residues 51−93)

contains a repeated sequence of eight residues [PH(Q)-GGGWGQ]. The backbone resonances for corresponding residues have degenerate chemical shift values (*13*); the NOE, T_1, and T_2 values used for these residues therefore represent a mean in each case. The relaxation behavior of the residues within and immediately adjacent to the octarepeat region is very similar.

Comparison of relaxation times determined by fitting decay curves to a two- or three-parameter equation indicated no significant difference in the relaxation times obtained for residues in the structured core of the prion protein (residues 128−225). However, residues in the flexible termini of the prion proteins (residues 29−127 and 226−231) exhibited a statistically significant difference in the values obtained using a two- or three-parameter fit. A plot of residue number versus the intensity offset I_∞ (i.e., the intensity of the peak at $t = \infty$) was used to identify a large systematic error in the estimation of the offset for intense peaks. This error occurs for both T_1 and T_2 data, even though the T_1 decay curves were recorded to more than three time constants for all residues. Very weak peaks can also give significant differences in relaxation rates determined using a two- or three-parameter fit. In these cases, a small offset from zero can make a significant contribution to the decay curve, so a three-parameter fit was used. The relaxation properties for the two PrP fragments are very similar for residues 100−231. The R_1 rates are relatively invariant with values ranging between 1.7 and 1.4 s^{-1}. Typical R_2 rates in the N-terminal portion of PrP, residues 29−120, are ∼4 s^{-1}, while in the C-terminal portion, rates of 18 s^{-1} are more typical. As with the R_2 data, the heteronuclear NOE values vary dramatically between the N- and C-terminal halves of the molecule. Negative steady-state heteronuclear NOE values are observed for residues 29−124 and positive values, in general greater than 0.6, for residues 135−220. The R_2 rate for residue G131 is 25−30 ms^{-1} for both PrP(29−231) and PrP(90−231). This is considerably larger than the values observed for other residues in PrP. Residues with unusually large R_2 rates (large line widths) are good candidates for possessing slow segmental motions. Residue L130 is overlapped with other resonances, and its relaxation properties could not be determined. The T_1 and T_2 relaxation data and the heteronuclear NOE data were also measured at 600 MHz for PrP-(29−231); similar trends in the values were observed (data not shown).

It is perhaps not surprising that the general trend in the relaxation behavior is similar in the two fragments of PrP, as the structure of the common regions of the two proteins is similar (*13*). However, one might have expected the T_2 relaxation time for the larger fragment to be shorter, reflecting a longer rotational correlation time. Surprisingly, the T_1/T_2 ratio, which reflects rotational diffusion of the fragments, is quite similar. It appears that the additional 60 residues in the unstructured N-terminal region of the larger fragment have only a relatively small effect on the effective rotational correlation time of residues in the folded core. However, the transverse relaxation is greatly affected by the presence of two domains with vastly different correlation times; this difference considerably complicates the interpretation of the relaxation data (see a later section). Relaxation data for the PrP(90−231) fragment have recently been reported, but no detailed analysis of the data was performed (*38*). Very similar R_1, R_2, and heteronuclear NOE values were observed in the two studies.

Reduced Spectral Density Mapping. The reduced spectral density function, $J(\omega)$, provides insights into the motion of the N−H bond vector at three frequencies, ω_0, ω_N, and $0.87\omega_H$. The reduced spectral density functions for both PrP-(90−231) and PrP(29−231) are shown in Figure 2. In general, the largest values for $J(0)$ are ∼6 ns for the C-terminal portion of the protein, indicating slow global tumbling typical for a structured protein. A single residue, G131, has a $J(0)$ spectral density value between 8 and 9 ns, which is much larger than typical values in the structured core of the protein (6 ± 0.5 ns), providing a clear indication that G131 is undergoing slow millisecond to microsecond time scale motions. The N-terminal regions of both constructs are very flexible, with $J(0)$ values of <1.5 ns for most residues in the region of residues 29−125. The $J(\omega_N)$ values show less variation with residue number, with typical values between 0.25 and 0.35 ns, although the structured C-terminal part of the protein gives generally higher values. The higher-frequency spectral density function $J(0.87\omega_H)$ has much smaller values (between 0.001 and 0.04 ns), and the trend is the opposite of that for $J(0)$, with larger values in the unstructured region and smaller values in the structured region.

Model Free Analysis of Dynamics. The dynamics of the prion molecule are complex, and we were unable to fit the ^{15}N relaxation data for PrP(29−231) and PrP(90−231) using the conventional model free approach (*31*, *32*). Attempts were made to fit the data with a single global correlation time (*33*). In addition, we tried to fit the data for each individual $^{15}N-^{1}H$ vector independently, i.e., to determine the effective rotational correlation time ($\tau_{c,i}$), the order parameter (S_i^2), and the internal correlation time ($\tau_{e,i}$) for each residue. Using simulated data, this approach has been shown to compensate for anisotropic tumbling in proteins (*39*), and it can be applied to unfolded proteins which do not exhibit a single global rotational correlation time (*40*, *41*). In the case of the prion protein fragments, the relaxation data could not be fitted by either approach, as indicated by the observation of S^2 values exceeding the theoretical maximum value of 1 for many residues in the globular domain [18 residues in PrP(29−231) and 32 residues in PrP(90−231)]. Estimation of S^2 directly from $J(0)$ and $J(\omega N)$ using eqs 6 and 7 also resulted in S^2 values greater than unity.

The problem appears to lie in the estimation of the rotational correlation time from the experimental T_1 and T_2 relaxation times. The average values of $\tau_{c,i}$ for residues in the three helices range from ∼12 (helix A) to ∼14 ns (helix C). In marked contrast, when the effective rotational correlation time for each helix is estimated from only T_1 and $\{^1H\}-^{15}N$ NOE measurements at two fields (500 and 600 MHz), τ_m values of 3.5 and 4.5 ns are obtained for helices A and C, respectively. These correlation times are significantly shorter, and are closer to what would be expected for a globular domain of ∼100 residues (*30*). The experimental T_2 values for amides in the globular core appear to be much too short relative to the values of T_1, which lead to an overestimate of τ_m. Systematic experimental errors in T_2 can be ruled out since similar T_2 values were obtained in measurements made for PrP(29−231) at both 500 and 600 MHz and for PrP(90−231) at 500 MHz. Further, comparable

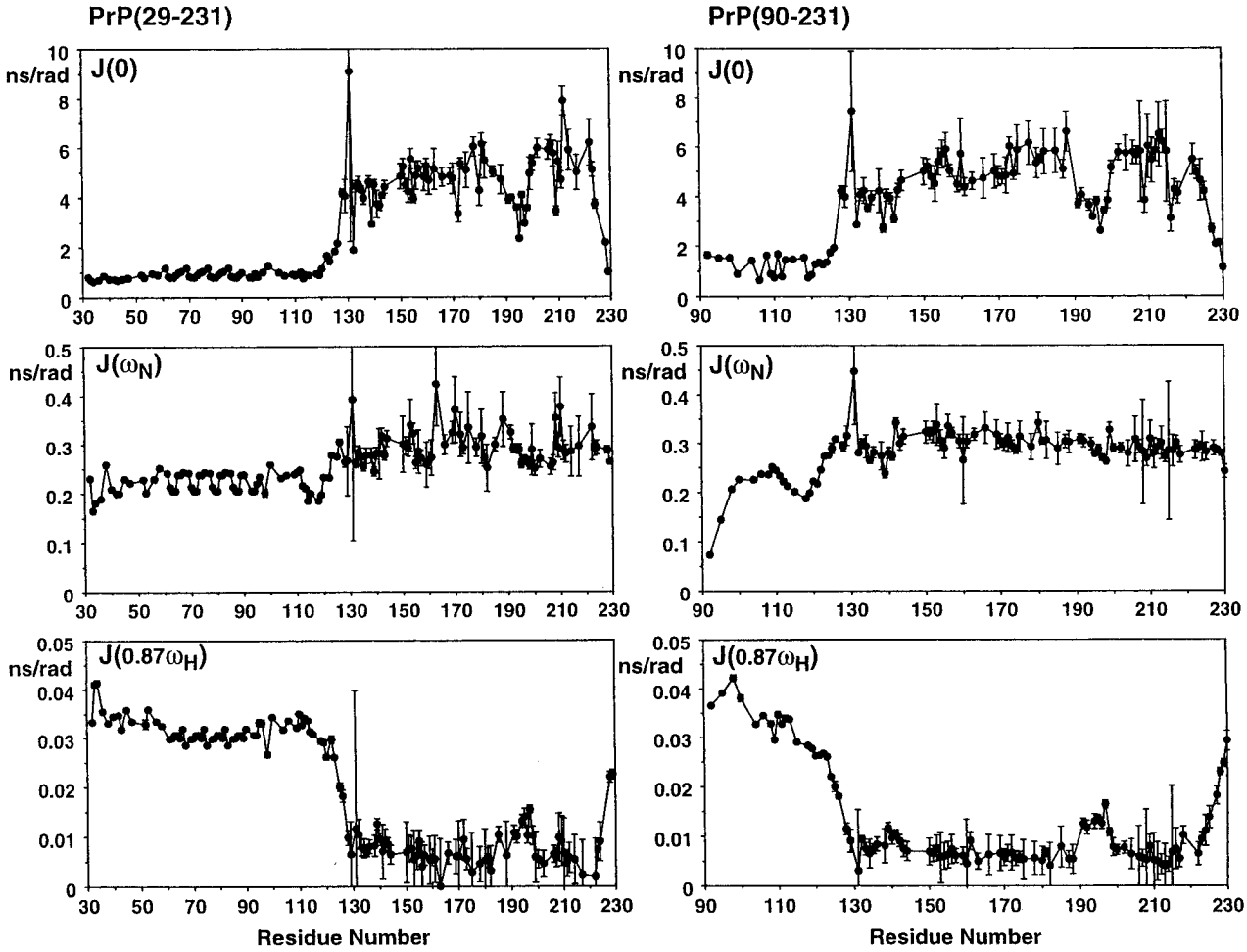

FIGURE 2: Reduced spectral density functions $J(0)$, $J(\omega_N)$, and $J(0.87\omega_H)$, calculated from the data depicted in Figure 1 for PrP(29−231) and PrP(90−231) at 500 MHz.

T_2 relaxation times were obtained in independent studies of PrP(90−231) by James and co-workers (*38*), who also noted that they were unable to fit the relaxation data using the model free approach.

Why are the experimental T_2 values systematically too short? This is not simply a consequence of anisotropic molecular tumbling (see a later section). Nor does it appear to be due to protein aggregation. Ultracentrifugation studies of PrP(90−231) yielded an association equilibrium constant of 0.054 mM^{-1} (*42*); thus, the population of dimer would be negligibly small at the concentration used for the NMR relaxation measurements (0.5 mM). We also note that while association would explain the large τ_c values calculated for the core from the T_1/T_2 ratio, it would not explain the failure to fit the data to physically meaningful values of S^2, nor would it explain the small τ_m determined from the T_1 and heteronuclear NOE values. Finally, we consider it unlikely that the anomalously short T_2 values arise from a slow (microsecond to millisecond) time scale conformational exchange process since all residues in the structured core are affected. Furthermore, reduction of T_2 by pervasive conformational fluctuations on a slow time scale can be definitively ruled out by $T_{1\rho}$ measurements. T_2 values calculated from the experimental $T_{1\rho}$ values are independent of spin lock field strength (data not shown) for residues in the protein core, showing that conformational exchange processes contribute insignificantly to the T_2 relaxation of most residues. A more likely explanation for the anomalously small T_2s is that the motions of the globular PrP core cannot be described by a simple anisotropic tumbling model with a unique diffusion tensor, i.e., with discrete values of τ_m parallel and perpendicular to the principal diffusion axis. This is not surprising, since tumbling of the globular domain will undoubtedly be influenced by the long, disordered N-terminal tail (residues 29−126 or 90−126) to which it is attached. Thus, the motions of individual N−H vectors are probably better characterized by a distribution of correlation times on a nanosecond time scale, reflecting the conformational disorder of the N-terminal region. Such an approach is frequently used to interpret the relaxation behavior of flexible polymers (*43*) and has recently been applied to unfolded proteins (*44*). Indeed, computer simulations show that even a modest distribution of correlation times leads to a large increase in $J(0)$ and a corresponding decrease in T_2, while T_1 and the $\{^1H\}-^{15}N$ NOE are much less affected (data not shown). Thus, the anomalous T_2 values observed for PrP(29−231) and PrP(90−231) are probably a consequence of the presence of the disordered N-terminal tail. Since the relaxation data cannot be interpreted using the model free approach to derive physically meaningful motional parameters, we restrict the analysis to a more qualitative one based on interpretation of the spectral densities. Spectral density mapping makes no assumptions about the nature of the rotational diffusion. Since $J(\omega_N)$ and $J(\omega_H)$ are independent

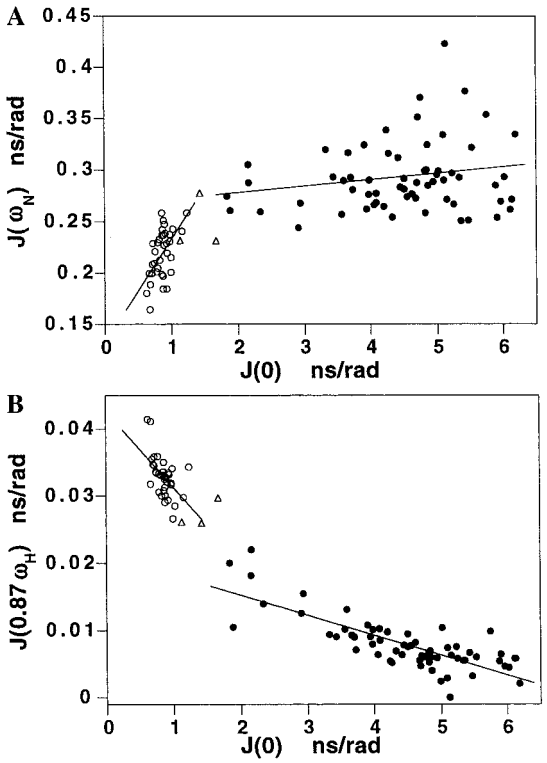

FIGURE 3: Values of (A) $J(\omega N)$ and (B) $J(0.87\omega H)$ plotted against the $J(0)$ value for the corresponding residue. Residues in the C-terminal domain [residues 125−231 (●)] and in the N-terminal domain [residues 29−119 (○)] show different linear correlation in each case. The solid lines were calculated using a linear least-squares fit to these data. Data points represented by △ occur in the transition region between the structured core and the flexible N-terminus (residues 120−123) and were not included in either of the linear least-squares fits.

of T_2 and are much less sensitive than $J(0)$ to the distribution of correlation times (simulations not shown), they provide reliable insights into the internal dynamics of PrP. Although $J(0)$ is very sensitive to the distribution of correlation times, it appears to be scaled uniformly so that relative differences in $J(0)$ still give qualitative information about backbone motions. This is demonstrated by the expected linear correlation of $J(0)$ with $J(\omega_N)$ and $J(0.87\omega_H)$, within each domain of PrP^C (Figure 3). Figure 3 also emphasizes the markedly different dynamic behaviors of the unstructured N-terminal domain and the folded core region of the protein.

Anisotropic Rotational Diffusion. An estimate was made of the anisotropy of the rotational diffusion of PrP^C. Hydrodynamic analysis of the structured core, residues 120−231 [utilizing the coordinates of the NMR structure of PrP(90−231) (*12*)], indicates that PrP(120−231) is by no means an isotropic sphere. The long axis (R_z) is 24 Å in length, and two shorter axes, R_x and R_y, are 16 and 12 Å, respectively. Calculation of the angle (θ) made by each N−H bond relative to the long axis of the molecule indicates that the N−H bonds within helix C are aligned with the long axis of the molecule, while helix A is approximately perpendicular to the long axis.

The anisotropic nature of the rotational diffusion should be reflected in the variation of the T_1/T_2 ratio for each residue when plotted against $(3\cos^2\theta - 1)/2$ (*36*). Such a plot is shown in Figure 4 for both PrP(29−231) and PrP(90−231); only the more rigid ^{15}N nuclei (heteronuclear NOE > 0.7)

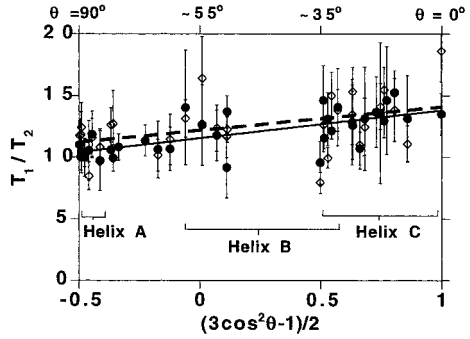

FIGURE 4: T_1/T_2 ratio vs $(3\cos^2\theta - 1)/2$ for each N−H bond relative to the estimated long axis of PrP. T_1/T_2 ratios for the structured regions of the protein (heteronuclear NOE > 0.7) are shown for (●) PrP(90−231) and (○) PrP(29−231). Locations of values for residues in the three helices are also indicated.

are shown. From Figure 4, it is clear that when the N−H bond is aligned with the long axis ($\theta = 0°$), a T_1/T_2 ratio of 14 is typical, while if the N−H bond is perpendicular to the long axis ($\theta = 90°$), a T_1/T_2 ratio of 10 is more typical.

Figure 4 suggests that both PrP(29−231) and PrP(90−231) tumble anisotropically, as there is a decrease in the T_1/T_2 ratio for each of these proteins with θ. The extent of the anisotropy for the two fragments is similar. Figure 4 also indicates the locations of the residues in each of the helices; it is clear that the values for each helix lie close to those expected from a simple consideration of the anisotropy of the core. The presence of an additional unstructured 61 residues in PrP(29−231) has almost no effect on the rate of rotational diffusion or on the extent of anisotropy in the tumbling. The long axis calculated from the structure of the core (residues 120−231) can only be an approximation to the long axis of PrP(90−231) or PrP(29−231). However, the T_1/T_2 ratio increases linearly with $(3\cos^2\theta - 1)/2$, strongly suggesting that the long axes of the two proteins do indeed follow approximately the direction of helix C, which at 27 residues is the longest of the three helices in PrP^C. Calculation of the rotational correlation time using only T_1 and the heteronuclear NOE data also reflects the anisotropic nature of the protein; the behavior of residues in helix C indicates a rotational correlation time of 4.5 ns, while residues in helix A appear to experience a correlation time of 3.5 ns.

Translational Diffusion. The translational diffusion coefficient (D_t) of PrP(29−231) was measured using pulsed field gradient methods (*25*) at three concentrations, 0.20, 0.30, and 0.38 mM. A sample data set is shown in Figure 5A for a protein concentration of 0.2 mM. The plot of ln(I) versus (gradient strength)^2 is linear over the range of field strength that was used. This is true for all three concentrations of PrP, and for a lysozyme standard, as shown in Figure 5B. The D_t for PrP(29−231) is independent of concentration within the uncertainties of the experiment, with an average value of $(0.78 \pm 0.03) \times 10^{-6}$ cm^2 s^{-1}.

The lack of significant variation of D_t with concentration suggests that PrP exists as a monomer under these conditions in solution. Similar experiments with PrP(90−231) also indicate a lack of concentration dependence of the translational self-diffusion coefficient between 0.1 and 1 mM (*38*). The mean D_t value for PrP^C(29−231) is small for a 22 kDa globular protein. Using the known hydrodynamic radius of

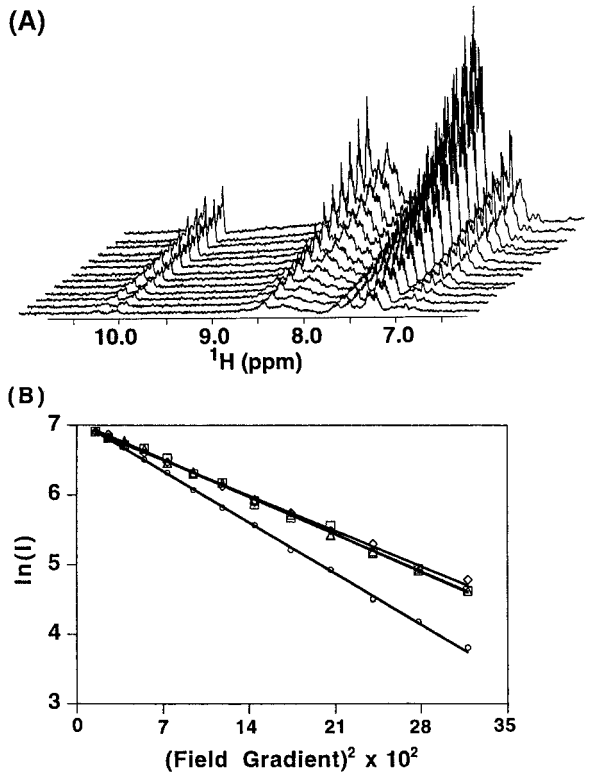

FIGURE 5: (A) Stacked plot of LED one-dimensional ^{1}H spectra for 0.2 mM PrP(29−231). (B) Translational diffusion measurements at concentrations of 0.2 (△), 0.3 (□), and 0.38 mM (◇) for PrP-(29−231) and for a 2 mM lysozyme standard (○). The natural log of the peak intensity [ln(*I*)] is plotted vs the square of the field gradient.

lysozyme [R_h = 20.5 Å (*45*)] as a reference, R_h of PrP^C(29−231) is estimated to be 28 Å. Using the empirical relationship $R_h = 4.75N^{0.29}$ (*45*), the hydrodynamic radius of the globular 102-amino acid core of PrP^C is estimated to be ∼18 Å. The greatly increased R_h determined from the diffusion measurements for the full-length protein undoubtedly reflects the influence of the unstructured N-terminal region on the hydrodynamic properties of the protein.

DISCUSSION

Backbone Flexibility of PrP(29−231) and PrP(90−231). The reduced spectral density functions, $J(0)$, $J(\omega_N)$, and $J(0.87\omega_H)$, that can be derived from relaxation parameters T_1, T_2, and {^{1}H}−^{15}N NOE provide different information about the motions of the polypeptide chain. The spectral density function at zero frequency is sensitive both to internal motions on the nanosecond time scale that are faster than the overall tumbling of the protein and to slow motions on the millisecond to microsecond time scale. In contrast, high-frequency spectral densities $J(0.87\omega_H)$ are sensitive only to fast internal motions, on a picosecond time scale. Typically, residues in PrP with restricted motion are dominated by nanosecond time scale motions and have large $J(0)$ and small $J(0.87\omega_H)$ values, while the reverse is true for more flexible regions of the backbone (Figure 2). The global rotational diffusion of both PrP fragments has a rate which makes $J(\omega_N)$ less sensitive to variations in internal motions, although this parameter does reflect the overall difference in the time scales of motions in the structured core of the protein and the tail.

Large high-frequency spectral densities, $J(0.87\omega_H)$, reflect fast internal picosecond motions. Spectral densities of <7.5 ps/rad indicate a relative lack of internal flexibility. This inflexibility is exhibited by much of helices B and C (Figure 2) as well as the extended coil region (residues 157−171) between helices A and B. Residues that exhibit spectral density between 7.5 and 15 ps/rad possess significant internal flexibility, and these include the flexible loop between helices B and C and the extended sequence preceding helix A. The residues between positions 29 and 126 exhibit $J(0.87\omega_H)$ spectral densities of >15 ps/rad and have marked flexibility. Recently published MD simulations have also identified regions with picosecond time scale fluctuations (*46*).

Figure 2 shows that the $J(0)$ values for the corresponding residues in the two fragments are very similar, indicating that the local motions of the protein backbone of residues 90−231 of the protein are similar in both PrP(90−231) and PrP(29−231). It is of interest that residues in the C-terminal portion of helix C (residues 216−222) have slightly reduced $J(\omega H)$ values for the longer fragment, commensurate with increased $J(0)$ values relative to the shorter fragment [PrP-(90−231)]. This suggests that the long N-terminal tail in PrP-(29−231) contributes to the stability of this region, which was also suggested (*15*) as the cause of an increased helical propensity in helix C in the full-length human prion protein. Chemical shift differences have also been observed for residues 187−193 of the Syrian hamster protein, suggesting that transient interactions between the long tail of PrP(29−231) and the structured core stabilizes helical structure in helix B (*13*). Similar chemical shift differences were observed for human PrP^C (*15*).

For PrP(29−231), the $J(0)$ values for residues 29−124 are very small (<1.5 ns/rad), while the $J(\omega_H)$ values are large. The hydrophobic cluster of residues 113−128 shows a number of long-range proton−proton NOEs, suggesting that at least transitory tertiary contacts occur in this region even though no regular secondary structure is present (*12*). Since this region has very low $J(0)$ values (<2 ns/rad) and large $J(0.87\omega_H)$ values, the tertiary packing in this region must be very short-lived.

The $J(0)$ values for PrP(90−231) (Figure 2) are shown mapped onto the structure of PrP(90−231) (*12*) in Figure 6. The central portions of helices B and C (residues 174−189 and 201−215) show the lowest flexibility on a microsecond to millisecond time scale [$J(0)$ > 5.5; blue backbone]. This is understandable in light of the presence of the disulfide bond between residues 179 and 214. Relatively large $J(0)$ values are also seen for residues at the C-terminus of helix A and in the loop connecting it to the second β-strand. These areas are in direct contact with the core region of helices B and C, whereas the remainder of the A helix, β-strands, and connecting loops are more flexible. The extended polypeptide chain between helices A and B (residues 156−173), which includes a very short stretch of β-strand (residues 161−164), shows increased mobility, and the other strand of the β-sheet is much more flexible with $J(0)$ values of ∼4 ns/rad, with the exception of G131 which shows exchange broadening (see below). The four residues on the C-terminal portion of helix B and the loop region between helices B and C (residues 190−198) show a marked flexibility, with $J(0)$ values between 3.0 and 4.0 ns/rad and large values of $J(\omega_H)$. The extended polypeptide structure from residues 128−144

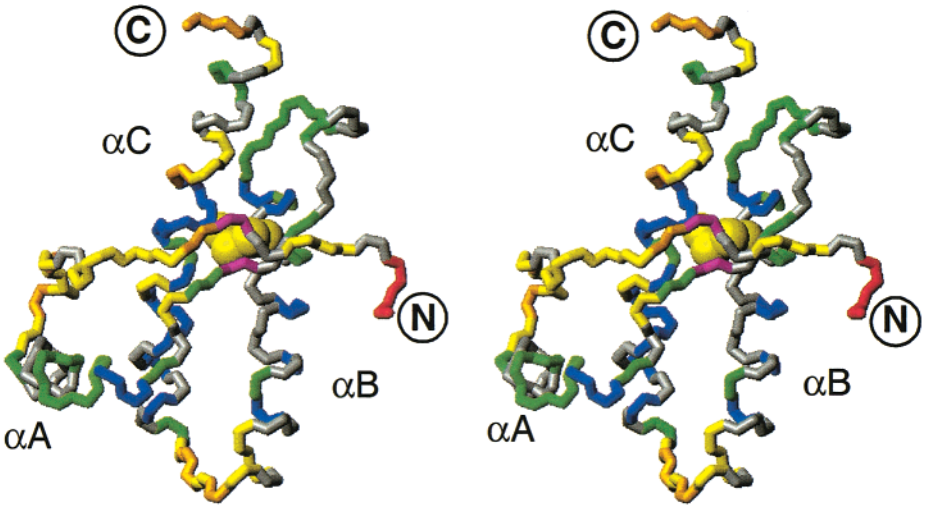

FIGURE 6: $J(0)$ values for PrP(90−231) (Figure 2), mapped onto the structure of PrP(90−231) (*38*). Residues for which $J(0) < 2.0$ are shown in red, $2.0 < J(0) < 3.5$ in orange, $3.5 < J(0) < 4.5$ in yellow, $4.5 < J(0) < 5.5$ in green, and $J(0) > 5.5$ in blue. β-Sheet residues G131 and V161 that show evidence of conformational exchange are highlighted in magenta. The figure was generated using the program MolMol (*57*).

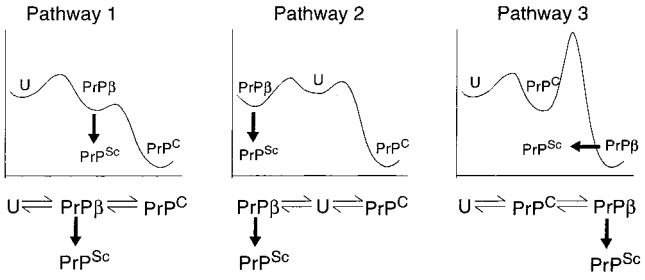

FIGURE 7: Schematic representation of the possible pathways by which the amyloid form of PrP (PrP^{Sc}) could be formed from a β-sheet-containing precursor $PrP\beta$ which also contains helices B and C. PrP^C is the cellular isoform containing helices A−C. U represents globally unfolded PrP.

also shows flexibility [$J(0) \sim 4.0$ ns/rad]. The C-terminal half of helix C, residues 215−224, also shows significantly increased flexibility, with a $J(0)$ of ~4.0 ns/rad for residues 216−219.

The unusually large $J(0)$ value of 9 ns/rad for G131 (magenta in Figure 6) indicates the presence of significant line broadening due to intermediate chemical exchange. Residue G131 forms part of the very short antiparallel β-sheet, residues 129−131 and 161−163. Resonances for residues in the other half of the antiparallel β-sheet do not exhibit such marked broadening, but the amide chemical shifts for V161 exhibit chemical exchange on an even slower time scale; two sets of resonances are found for V161, with the populations of the two conformers varying depending on subtle differences in solution conditions. This behavior was also noted by Liu et al. (*38*).

Solution structures of four mammalian prion proteins are now available: Syrian hamster (*12*, *13*, *38*), mouse (*11*, *14*, *47*, *48*), cow (*49*), and human (*15*). As would be expected from the high degrees of sequence homology, the basic fold is similar in all four. However, there are some variations in the stability and flexibility of the backbone. In particular, the resonances of the loop between the second β-strand and helix B (residues 169−171) are not observed in the mouse and human proteins, due to conformational exchange. No evidence for conformational exchange is observed in the Syrian hamster protein, either in the structures (*38*) or in the dynamics (this work). This region is the putative binding site for protein X (*16*). The range of flexibility that PrP^C possesses is extremely variable even in the structured C-terminal domain, where the $J(0)$ values range between 3 and 6.5. This range of flexibility clearly reflects the inherent conformational plasticity of parts of PrP^C, which has previously been noted under various solution conditions (*42*).

Implications of Conversion of PrP^C to PrP^{Sc} for Prion Disease. The mechanism by which PrP^C converts into pathogenic PrP^{Sc} is fundamental to understanding prion diseases. It is thought that the conversion proceeds via a conformational switch between a highly helical PrP^C and a monomeric isoform rich in β-sheet (*9*), which we term PrP_β. The monomeric species PrP_β can form multimeric PrP^{Sc} and higher-order aggregates which are infectious.

Several folding pathways can be envisaged for the conversion of PrP^C to PrP^{Sc} via PrP_β (Figure 7). In all of these pathways, PrP_β, once formed, can add to an existing oligomeric PrP^{Sc} or perhaps join other monomers to form a new oligomer of PrP^{Sc}. In pathway 1, PrP_β is a folding intermediate for the formation of PrP^C. In pathway 2, the formation of PrP_β is off-pathway, and it may contain no structural elements found in PrP^C. It is difficult to reconcile either of these pathways with the observation that PrP^C and the multimeric form PrP^{Sc} can coexist in infected animal brains while only PrP^C is found in normal animals. Alternatively (pathway 3), PrP^C may be a kinetically trapped intermediate on the folding pathway to PrP_β and PrP^{Sc}, which ought to contain recognizable structural elements similar to those of PrP^C (*50*, *51*).

If PrP^C converts to PrP_β and PrP^{Sc} via pathway 3, then an understanding of the inherent flexibility of PrP^C should give us clues about the likely locations of regions of the structure most amenable to rearrangement. Residues with greater flexibility [smaller $J(0)$ values and larger $J(\omega_H)$ values] have a lower enthalpy barrier during a structural rearrangement, and therefore, these are the residues that seem most likely to be involved in the conformational switch to PrP_β. A variety of previous antibody binding and peptide conformational

studies also localize the structural difference between PrP^C and PrP^{Sc} to residues 90−145 (*42*, *50*, *52*).

Spectral density functions, in particular $J(0)$, indicate that the central portions of helices B and C are least flexible and are therefore the most likely regions of the protein to remain helical during the conversion of PrP^C. Consistent with this hypothesis, the integrity of the disulfide bond between Cys179 and Cys214 has been shown to be necessary for PrP infectivity (*53*, *54*). FTIR spectroscopy and thin film CD have been used to obtain approximate ratios of the secondary structure content of the two forms of the protein (*9*, *10*). These measurements suggest a 20−30% helix content and 34−43% β-sheet content for PrP^{Sc}(23−231). A 20−30% helical content of PrP(23−231) is equivalent to residues 41−62 in helix. Since helices B and C contain a total of 48 residues, this is consistent with the presence of significant portions of intact helical structure in helices B and C in PrP^{Sc}.

Studies with antibodies, which have been mapped to various epitopes on PrP (*52*), also support the hypothesis that a core of the molecule containing helices B and C remains intact after the conversion of PrP^C to PrP^{Sc}. A "miniprion" construct known as PrP106, which lacks residues 23−89 and 141−176, still causes prion propagation in transgenic mice (*54*, *55*). This construct presumably retains helical structure in helices B and C, which span residues 172−227 in the wild-type protein. As noted previously (*46*, *48*), a significant fraction of the mutations in human PrP associated with disease is likely to destabilize the packing of helices B and C to the rest of the protein. In particular, the D178N mutation breaks the salt bridge with R164, which is involved in the packing of helix B with β-strand S2. The T183A mutation eliminates the hydrogen bond between the side chains of T183 and W162, also in β-strand S2. The R208H mutation eliminates a salt bridge to residues E164 and D144 that stabilizes the packing between helices A and B. Regions of increased flexibility [reduced $J(0)$] within helix C also appear to be involved in contacts with the β-strands. If we assume that the rearrangement of the β-strands is a key event in the formation of PrP_β and PrP^{Sc} from PrP^C, then mutations which destabilize helix C could also destabilize the β-structure of PrP^C and trigger the transition.

It is clear that a range of studies supports the conclusion from our relaxation measurements that a structured core containing at least the central portions of helices B and C, joined by the disulfide bond between residues 179 and 214, is likely to constitute part of the PrP^{Sc} structure. The remaining part of the protein, N-terminal to this structured core, has presumably rearranged in PrP^{Sc}. The monomeric β-rich isoform PrP_β may contain either unstructured or β-type conformation in the region between residues 90 and 140. The relaxation measurements indicate that this region has significantly increased mobility on several time scales relative to the helix B−helix C core. This would facilitate conversion of this region into β-sheet, either in the monomer itself or upon binding to the PrP^{Sc} template. Structure prediction of PrP^{Sc} based on helical propensities also suggests that the helix B−helix C region should adopt helical structure, with residues 90−140 forming β-sheet structure (*56*). In addition, the observation of slow time scale conformational fluctuations for residues in the β-sheet suggests that slow segmental motions, possibly unzipping of this sheet, may be part of the process of conversion of PrP^C to PrP_β.

ACKNOWLEDGMENT

We thank Darlene Groth for expression and labeling of PrP(29−231) and PrP(90−231) and Drs. Brendan Duggan, Ishwar Radhakrishnan, and Michael Osborne for stimulating discussions and for the use of programs for data analysis. We also thank Dr. John Chung for assistance with NMR experiments.

REFERENCES

1. Prusiner, S. B. (1997) *Science 278*, 245−251.
2. Prusiner, S. B. (1996) in *Fields Virology* (Fields, B. N., Knipe, D. M., and Howley, P. M., Eds.) pp 2901−2950, Lippincott-Raven Publishers, Philadelphia.
3. Horwich, A. L., and Weissman, J. S. (1997) *Cell 89*, 499−510.
4. Chazot, G., Broussolle, E., Lapras, C., Blattler, T., Aguzzi, A., and Kopp, N. (1996) *Lancet 347*, 1181−1181.
5. Will, R. G., Ironside, J. W., Zeidler, M., Cousens, S. N., Estibeiro, K., Alperovitch, A., Poser, S., Pocchiari, M., Hofman, A., and Smith, P. G. (1996) *Lancet 347*, 921−925.
6. Alper, T., Cramp, W. A., Haig, D. A., and Clarke, M. C. (1967) *Nature 214*, 764−766.
7. Prusiner, S. B. (1982) *Science 216*, 136−144.
8. Prusiner, S. B. (1991) *Science 252*, 1515−1522.
9. Pan, K.-M., Baldwin, M., Nguyen, J., Gasset, M., Serban, A., Groth, D., Mehlhorn, I., Huang, Z., Fletterick, R. J., Cohen, F. E., and Prusiner, S. B. (1993) *Proc. Natl. Acad. Sci. U.S.A. 90*, 10962−10966.
10. Safar, J., Roller, P. P., Gajdusek, D. C., and Gibbs, C. J., Jr. (1993) *J. Biol. Chem. 268*, 20276−20284.
11. Riek, R., Hornemann, S., Wider, G., Billeter, M., Glockshuber, R., and Wüthrich, K. (1996) *Nature 382*, 180−182.
12. James, T. L., Liu, H., Ulyanov, N. B., Farr-Jones, S., Zhang, H., Donne, D. G., Kaneko, K., Groth, D., Mehlhorn, I., Prusiner, S. B., and Cohen, F. E. (1997) *Proc. Natl. Acad. Sci. U.S.A. 94*, 10086−10091.
13. Donne, D. G., Viles, J. H., Groth, D., Mehlhorn, I., James, T. L., Cohen, F. E., Prusiner, S. B., Wright, P. E., and Dyson, H. J. (1997) *Proc. Natl. Acad. Sci. U.S.A. 94*, 13452−13457.
14. Riek, R., Hornemann, S., Wider, G., Glockshuber, R., and Wüthrich, K. (1997) *FEBS Lett. 413*, 282−288.
15. Zahn, R., Liu, A., Luhrs, T., Riek, R., Von Schroetter, C., Lopez, G. F., Billeter, M., Calzolai, L., Wider, G., and Wuthrich, K. (2000) *Proc. Natl. Acad. Sci. U.S.A. 97*, 145−150.
16. Kaneko, K., Zulianello, L., Scott, M., Cooper, C. M., Wallace, A. C., James, T. L., Cohen, F. E., and Prusiner, S. B. (1997) *Proc. Natl. Acad. Sci. U.S.A. 94*, 10069−10074.
17. Mehlhorn, I., Groth, D., Stockel, J., Moffat, B., Reilly, D., Yansura, D., Willett, W. S., Baldwin, M., Fletterick, R., Cohen, F. E., Vandlen, R., Henner, D., and Prusiner, S. B. (1996) *Biochemistry 35*, 5528−5537.
18. Van Geet, A. L. (1970) *Anal. Chem. 42*, 679−680.
19. Farrow, N. A., Muhandiram, R., Singer, A. U., Pascal, S. M., Kay, C. M., Gish, G., Shoelson, S. E., Pawson, T., Forman-Kay, J. D., and Kay, L. E. (1994) *Biochemistry 33*, 5984−6003.
20. Zinn-Justin, S., Berthault, P., Guenneugues, M., and Desvaux, H. (1997) *J. Biomol. NMR 10*, 363−372.
21. Stone, M. J., Fairbrother, W. J., Palmer, A. G., III, Reizer, J., Saier, M. H., Jr., and Wright, P. E. (1992) *Biochemistry 31*, 4394−4406.
22. Mandel, A. M., Akke, M., and Palmer, A. G., III (1995) *J. Mol. Biol. 246*, 144−163.
23. Farrow, N. A., Zhang, O., Szabo, A., Torchia, D. A., and Kay, L. E. (1995) *J. Biomol. NMR 6*, 153−162.
24. Tjandra, N., Wingfield, P., Stahl, S., and Bax, A. (1996) *J. Biomol. NMR 8*, 273−284.
25. Altieri, A. S., Hinton, D. P., and Byrd, R. A. (1995) *J. Am. Chem. Soc. 117*, 7566−7567.
26. Barbato, G., Ikura, M., Kay, L. E., Pastor, R. W., and Bax, A. (1992) *Biochemistry 31*, 5269−5278.

27. Peng, J. W., and Wagner, G. (1995) *Biochemistry 34*, 16733−16752.
28. Farrow, N. A., Zhang, O., Forman-Kay, J. D., and Kay, L. E. (1995) *Biochemistry 34*, 868−878.
29. Lefèvre, J. F., Dayie, K. T., Peng, J. W., and Wagner, G. (1996) *Biochemistry 35*, 2674−2686.
30. Dayie, K. T., Wagner, G., and Lefèvre, J.-F. (1996) *Annu. Rev. Phys. Chem. 47*, 243−282.
31. Lipari, G., and Szabo, A. (1982) *J. Am. Chem. Soc. 104*, 4559−4570.
32. Lipari, G., and Szabo, A. (1982) *J. Am. Chem. Soc. 104*, 4546−4559.
33. Bracken, C., Carr, P. A., Cavanagh, J., and Palmer, A. G., III (1999) *J. Mol. Biol. 285*, 2133−2146.
34. Fushman, D., Weisemann, R., Thüring, H., and Rüterjans, H. (1994) *J. Biomol. NMR 4*, 61−78.
35. Tjandra, N., Feller, S. E., Pastor, R. W., and Bax, A. (1995) *J. Am. Chem. Soc. 117*, 12562−12566.
36. Lillemoen, J., and Hoffman, D. W. (1998) *J. Mol. Biol. 281*, 539−551.
37. Lee, L. K., Rance, M., Chazin, W. J., and Palmer, A. G. (1997) *J. Biomol. NMR 9*, 287−298.
38. Liu, H., Farr-Jones, S., Ulyanov, N. B., Llinas, M., Marqusee, S., Groth, D., Cohen, F. E., Prusiner, S. B., and James, T. L. (1999) *Biochemistry 38*, 5362−5377.
39. Schurr, J. M., Babcock, H. P., and Fujimoto, B. S. (1994) *J. Magn. Reson., Ser. B 105*, 211−224.
40. Yang, D. W., Mok, Y. K., Forman-Kay, J. D., Farrow, N. A., and Kay, L. E. (1997) *J. Mol. Biol. 272*, 790−804.
41. Farrow, N. A., Zhang, O., Forman-Kay, J. D., and Kay, L. E. (1997) *Biochemistry 36*, 2390−2402.
42. Zhang, H., Stöckel, J., Mehlhorn, I., Groth, D., Baldwin, M. A., Prusiner, S. B., James, T. L., and Cohen, F. E. (1997) *Biochemistry 36*, 3543−3553.
43. Bovey, F. A., and Mirau, P. A. (1996) in *NMR of Polymers*, Academic Press, San Diego.
44. Buevich, A. V., and Baum, J. (1999) *J. Am. Chem. Soc. 121*, 8671−8672.
45. Wilkins, D. K., Grimshaw, S. B., Receveur, V., Dobson, C. M., Jones, J. A., and Smith, L. J. (1999) *Biochemistry 38*, 16424−16431.
46. Zuegg, J., and Gready, J. E. (1999) *Biochemistry 38*, 13862−13876.
47. Billeter, M., Riek, R., Wider, G., Hornemann, S., Glockshuber, R., and Wüthrich, K. (1997) *Proc. Natl. Acad. Sci. U.S.A. 94*, 7281−7285.
48. Riek, R., Wider, G., Billeter, M., Hornemann, S., Glockshuber, R., and Wüthrich, K. (1998) *Proc. Natl. Acad. Sci. U.S.A. 95*, 11667−11672.
49. Lopez, G. F., Zahn, R., Riek, R., and Wuthrich, K. (2000) *Proc. Natl. Acad. Sci. U.S.A. 97*, 8334−8339.
50. Cohen, F. E., and Prusiner, S. B. (1998) *Annu. Rev. Biochem. 67*, 793−819.
51. Prusiner, S. B., Scott, M. R., DeArmond, S. J., and Cohen, F. E. (1998) *Cell 93*, 337−348.
52. Peretz, D., Williamson, R. A., Matsunaga, Y., Serban, H., Pinilla, C., Bastidas, R. B., Rozenshteyn, R., James, T. L., Houghten, R. A., Cohen, F. E., Prusiner, S. B., and Burton, D. R. (1997) *J. Mol. Biol. 273*, 614−622.
53. Turk, E., Teplow, D. B., Hood, L. E., and Prusiner, S. B. (1988) *Eur. J. Biochem. 176*, 21−30.
54. Muramoto, T., Scott, M., Cohen, F. E., and Prusiner, S. B. (1996) *Proc. Natl. Acad. Sci. U.S.A. 93*, 15457−15462.
55. Cheetham, M. E., and Caplan, A. J. (1998) *Cell Stress Chaperones 3*, 28−36.
56. Huang, Z., Prusiner, S. B., and Cohen, F. E. (1996) *Curr. Top. Microbiol. Immunol. 207*, 49−67.
57. Koradi, R., Billeter, M., and Wüthrich, K. (1996) *J. Mol. Graphics 14*, 51−55.

BI002898A